

We are IntechOpen, the world's leading publisher of Open Access books Built by scientists, for scientists

4,800

Open access books available

122,000

International authors and editors

135M

Downloads

Our authors are among the

154

Countries delivered to

TOP 1%

most cited scientists

12.2%

Contributors from top 500 universities



WEB OF SCIENCE™

Selection of our books indexed in the Book Citation Index
in Web of Science™ Core Collection (BKCI)

Interested in publishing with us?
Contact book.department@intechopen.com

Numbers displayed above are based on latest data collected.

For more information visit www.intechopen.com



QSAR Analysis of Purine-Type and Propafenone-Type Substrates of P-Glycoprotein Targeting β -Amyloid Clearance

Jie Yang and Jie Chen

Additional information is available at the end of the chapter

<http://dx.doi.org/10.5772/54975>

1. Introduction

Therapy for central nervous system (CNS) diseases requires drugs that can cross the blood-brain barrier (BBB) (Cheng et al, 2010). BBB not only maintains the homeostasis of the CNS, but also refuses many potentially important diagnostic and therapeutic agents from entering into the brain (Chen et al, 2009). The pathogenesis of Alzheimer's disease (AD) senile plaque and neurofibrillary tangle lesions putatively involves a compromised BBB (Jevnes & Provias, 2011), which protects the brain against endogenous and exogenous compounds and plays an important part in the maintenance of the microenvironment of the brain (Vogelgesang et al, 2011). The ability of drug permeating across BBB becomes critical in the development of new medicines, especially in the design of new drugs which are active in brain tissue. In particular, the importance of brain-to-blood transport of brain-derived metabolites across the BBB has gained increasing attention as a potential mechanism in the pathogenesis of neurodegenerative disorders such as Parkinson's disease (Bartels, 2011) and AD characterized by the aberrant polymerization and accumulation of specific misfolded proteins, particularly β -amyloid ($A\beta$), a neuropathological hallmark of AD. P-glycoprotein (P-gp or MDR1/ABCB1) is a 170-kDa transmembrane protein widely expressed from the epithelial cells of the intestine, liver, kidney, placenta, uterus, and testis to endothelial cells of the BBB (Gottesman & Pastan, 1993). It belongs to the ABC (ATP-binding cassette) transporter family and serves to pump exogenous substances out of the cells (Suresh et al, 1999). The domain topology of P-gp consist of two homologous halves each consist a transmembrane domain preceding a cytosolic nucleotide binding domain. Each transmembrane domain is composed of six transmembrane α -helix segments involved in efflux as well as in drug binding (Kast et al, 1996). The ABC transport protein P-gp, a major component of the BBB, mediates the efflux of $A\beta$ from the brain as well as a major

factor in mediating resistance to brain entry by numerous exogenous chemicals, including therapeutic pharmaceuticals (Bendayan et al, 2002). P-gp plays a role in the etiology of AD through the clearance of A β from the brain. Some drugs, such as rifampicin, dexamethasone, caffeine, verapamil, hyperforin, β -estradiol and pentylentetrazole, were able to improve the efflux of A β from the cells via P-gp up-regulation (Abuznait et al, 2011). Meanwhile, some compounds have been shown to reverse the P-gp mediated multidrug resistance (MDR), including verapamil, adriamycin, cyclosporin, and dexverapamil (Kothandan et al, 2011). Harta et al (2010) have shown that up-regulate P-gp in the early stages of AD has the potential to increase A β clearance from the brain and reduce A β brain accumulation by a transgenic mouse model of AD (human amyloid precursor protein-overexpressing mice). Abuznait et al (2011) have also elucidated the impact of P-gp up-regulation on the clearance of A β , which indicated targeting A β clearance via P-gp up-regulation effective in slowing or halting the progression of AD and the possibility of P-gp as a potential therapeutic target for AD.

P-gp at the BBB functions as an active efflux pump by extruding a substrate from the brain, which is important for maintaining loco-regional homeostasis in the brain and protection against toxic compounds (Bartels, 2011). P-gp is also discovered in various resistant tumor cells and expressed widely in many normal tissues and plays a very important role in drug ADME-Tox (absorption, distribution, metabolism, excretion, and toxicity). MDR is a matter of growing concern in chemotherapy. Cells which express the multidrug resistance phenotype can over-express efflux transporters after exposure to a single agent. As a result, these cells become resistant to the selective agent and cross-resistant to a broad spectrum of structurally and functionally dissimilar drugs. The drug efflux pump P-gp has been shown to promote MDR in tumors as well as to influence ADME properties of drug candidates (Jabben et al, 2012). P-gp is expressed at the BBB, the blood-cerebrospinal fluid barrier, and the intestinal barrier, thus modulating the absorption and excretion of xenobiotics across these barriers. P-gp and its ligands (substrates and inhibitors) are therefore extensively studied both with respect to reversing MDR in tumors and for modifying ADME-Tox properties of drug candidates, such as CNS active agents (Jabben et al, 2012). P-gp possesses broad substrate specificity and substrates include members of many clinically important therapeutic drug classes, including anti-HIV protease inhibitors, calcium channel blockers used in the treatment of angina, hypertension, antibiotics and cancer chemotherapeutics (Stouch & Gudmundsson, 2002). In this active efflux process, energy originating from ATP hydrolysis is directly consumed. Because of such a wide distribution of P-gp, so if a drug such as quinidine or verapamil inhibits the function of P-gp, it will also inhibit the excretion of digoxin by P-gp leading to increased plasma levels and toxicity due to digoxin. It is believed to be an important protective mechanism against environmental toxins (Martin, 2004). Since the function of P-gp always results in lack of intracellular levels of the drug necessary for effective therapy, the overexpression of P-gp in certain malignant cells is always associated with MDR phenotype (Sharom, 1997). Although recently low resolution structure of P-gp is obtained, its physiological function and mechanisms of MDR modulation are still not very clear (Li et al, 2005). It is well known that a large number of structurally and functionally diverse compounds act as substrates or modulators of P-gp, including calcium and sodium channel blockers, calmodulin antagonists and structural analogues, protein kinase C inhibitors, steroidal and structurally related com-

pounds, indole alkaloids, cyclic peptides and macrolide compounds, flavanoids and miscellaneous compounds (Wang et al, 2003), which mostly share common structural features, such as aromatic ring structures and high lipophilicity. Some of them possess MDR reversing activity. But only a small number of them have entered clinical study and classification of candidate drugs as substrates or inhibitors of the carrier protein is of crucial importance in drug development (Wang et al, 2005).

On the other hand, the prerequisite to cure neurological disorders is that the drug distribution in CNS can reach effectively therapeutic concentrations (Chen et al, 2009). Usually, the high BBB penetration is needed for drugs that activate in brain. The molecule negotiating the BBB must go through cellular membranes comprising of a lipid bilayer. Until now, it is widely accepted that interaction of compounds with P-gp is a complex process and at this time the details of its mechanism of action are still the subject on hot debate. Although the experimental analysis of drug permeability is essential but the procedure of experiment is time consuming and complicated, a theoretical model of drug permeability is effective to give predictions. Membrane-interaction (MI)-QSAR (quantitative structure-activity relationship) method is a structure-based design methodology combined with classic intramolecular QSAR analysis to model chemically and structurally diverse compounds interacting with cellular membranes. Our modified MI-QSAR method that combines QSAR with solute-membrane-water complex simulating the BBB environment is more close to the body condition than MI-QSAR and possesses higher ability to predict organic compounds across BBB (Chen & Yang, 2006). Before we construct any QSAR models, several things should be consider seriously first. There are several critical assumptions that can influence validity and correctness of any QSAR study as follows: the same mechanism of action of all studied analogs; a comparable manner of their binding to the receptor; correlation of binding to the interaction energies; correlation of measured biological activities to the binding affinities (Kubinyi, 1995). All the accuracy answer and research based on the questions above may guarantee that proper and reliable relationships are obtained. However, in case of MDR modulators different mechanisms and different binding sites may be involved. Several screening assays can help in the identification of substrates and inhibitors although they have both advantages and drawbacks, such as cytotoxicity assays (Wiese & Pajeva, 2001), inhibition of efflux assays (Stouch & Gudmundsson, 2001), P-gp-ATPase activation assays, and drug transport assays (Taub et al, 2005).

The goal of a QSAR study is to find a means of predicting the activity of a new compound. If possible, a desirable goal is the understanding of the biology and chemistry that give rise to that activity and the consequential possibility of reengineering the compound to remove or enhance that activity. One successful example is the transformation of nalidixic acid with the help of QSAR into an important family of drug: the quinolone carboxylates, such as norfloxacin, fleroxacin, ciprofloxacin, and levofloxacin (Alka, 2003). Since the method was established in the 1960s, QSAR equations have been used to describe the biological activities of thousands of different drugs and drug candidates (Kuo et al, 2004). The method definitely provides a more accurate way to synthesize or filtrate the new chemical compounds. At last, the final destination is to degrade the cost of research and manufacture. To date, so many methods have been used in QSAR study and some of them have got successful results. There are general

methods used in the literatures these years, such as multiple linear regression (MLR) method, partial least square regression (PLSR) (Li et al, 2005), MI-QSAR analysis (Chen & Yang, 2006), and three-dimension (3D) QSAR (Cramer et al, 1988), and artificial neural network (ANN) (Chen et al, 2006). In order to get more accurate results and QSAR models, we have used two different analyses: MLR and PLSR. Moreover, we focus on constructing theoretical models of the interaction between organic compounds and P-gp as well as the predictive models of blood-brain barrier partitioning of organic compounds on the basis of QSAR analysis and MI-QSAR analysis.

2. Materials and methods

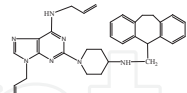
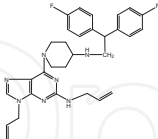
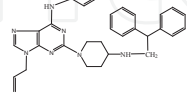
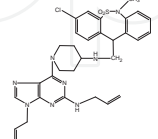
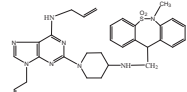
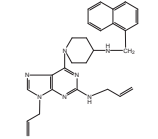
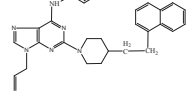
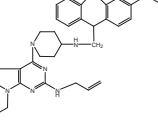
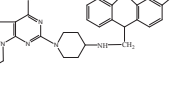
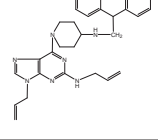
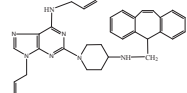
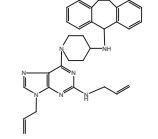
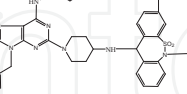
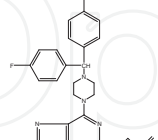
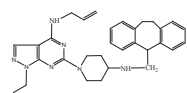
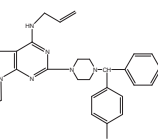
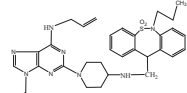
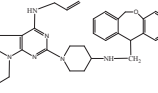
2.1. P-glycoprotein ligands

Building of some compounds 36 purine derivatives were selected and used in QSAR analysis (table 1) (Dhainaut et al, 1996). These compounds were divided into two sets: the training set and the test set. The study of the MDR-reversing properties of these derivatives was carried out in vitro on P388/VCR-20 cells, a murine leukemia cell line whose resistance was induced by vincristine (VCR), and KB-A1 cells, a human epidermoid carcinoma cell line whose resistance was induced by adriamycin (ADR). The compounds were tested at four concentrations (0.5–5 μ M) in association with VCR (P388/VCR-20 cells) or ADR (KB-A1 cells). In this test, MDR ratio in P388/VDR-20 and KB-A1 in vitro was used as biological activity for the

whole dataset, namely $MDR_{ratio} = \frac{IC_{50}(CD)}{IC_{50}(CD + mod)}$. Here “CD” is the abbreviation for cytotoxic

drug (such as VCR and ADR) in cytotoxicity assays, and “mod” means modulators. It is defined as ratio between the IC_{50} values (concentration that inhibits the growth of MDR cells by 50%) of the cytotoxic agent in absence and presence of relatively nontoxic concentration of the modifier (Wiese & Pajeva, 2001). Most often the IC_{50} for several concentration of a cytotoxic drug is evaluated in the presence and absence of a nontoxic concentration of a P-gp modifier. In this assay modulators that interact with P-gp and thus, reduce the efflux of the cytotoxic compounds, will increase the apparent toxicity of the cytotoxic compound. It is important to keep in mind that it is based on a general assessment of cytotoxicity and thus may account for more than one acting mechanism in the resistant cells used (Stouch & Gudmundsso, 2001). Furthermore, it is well known that the MDR ratio for any given compound can vary greatly depending on the cell type used for the assay as well as the intrinsic cytotoxicity of the compounds used. The data is also dependent on the concentration of the P-gp substrates or modulators used in the studies (Ford et al, 1990).

Similarly, another 21 propafenone analogs were selected from the literature of Diethart Schmid et al (1999) and used in QSAR analysis (table 2). In this test K_a of P-gp ATPase in the adriamycin-resistant subline CCRF ADR5000 was used as biological activity for the whole dataset (Schmid et al, 1999). The assays were performed based on the colorimetric determination of inorganic phosphate released by the hydrolysis of ATP. Table 2 shows all the structures and the experimental biological activity value.

No.	Structure	in vitro reversal fold reversion (MDR ratio)		No.	Structure	in vitro reversal fold reversion (MDR ratio)	
		P388/ VCR-20	KB-A1			P388/VCR-20	KB-A1
A1		50	171	A19		36	49
A2		78	278	A20		70	214
A3		75	238	A21		35	113
A4		53	236	A22		133	200
A5		236	160	A23		193	189
A6		93	208	A24		24	142
A7		124	102	A25		13	6
A8		30	120	A26		24	9
A9		57	75	A27		84	406

No.	Structure	in vitro reversal fold reversion (MDR ratio)		No.	Structure	in vitro reversal fold reversion (MDR ratio)	
		P388/ VCR-20	KB-A1			P388/VCR-20	KB-A1
A10		108	136	A28		57	68
A11		37	44	A29		108	723
A12		15	83	A30		27	370
A13		78	272	A31		288	210
A14		56	147	A32		59	121
A15		75	152	A33		71	499
A16		51	209	A34		13	264
A17		70	171	A35		3	5
A18		129	156				

Note: Ratio of IC₅₀ (cytotoxic alone (VCR for P388/VCR-20, ADR for KB-A1 cells))/IC₅₀ (cytotoxic + modulator) (1 μM in association with VCR or 2.5 μM in association with ADR) (Dhainaut et al, 1996).

Table 1. The structures and MDR ratios of 35 purine derivatives in the training/test sets.

No.	Structure	Ka(μ M/L)	LogP	No.	Structure	Ka(μ M/L)	LogP
A36		3.34	3.39	A45		1.53	4.3
A37		5.3	3.62	A46		1.47	4.93
A38		2.59	3.67	A47		0.55	5.2
A39		122	1.42	A48		7.64	4.25
A40		0.36	4.93	A49		12.2	4.52
A41		6.13	2.67	A50		2.26	4.88
A42		120	0.94	A51		10.5	2.38
A43		18.5	2.54	A52		12.8	3.94
A44		1.01	3.98	A53		4.15	4.93

Table 2. The structures and Ka values and LogP of 18 propafenone analogs in the training/test sets.

Finally, all two-dimensional structures of these compounds mentioned above were constructed using the chemical drawing software ChemDraw 8.0 and prepared for the next calculation.

Calculation of some descriptors Molecular descriptors are “numbers that characterize a specific aspect of the molecular structure” (Karelson, 2000). There are a great number of molecular descriptors that can be used in QSAR studies in the structure parameterization form, which include physicochemical properties (such as hydrophobicity, aqueous solubility, molecular electronegativity, and molecular refractivity), quantum chemical parameters (i.g. atomic charges, energies of HOMO (highest occupied molecular orbital) and LUMO (lowest unoccupied molecular orbital)) (Karelson & Lobanov, 1996), topological indexes (i.e. molecular connectivity indexes) (Ponce et al, 2004), and other three-dimensional (3D) descriptors. Molecular descriptors were mostly calculated by the commercial software packages Chemoffice Chem3D Ultra 8.0, which included molecular mechanism parameters (Bending Energy (E_{bend}), Stretch-Bend Energy (E_{stretch}), Torsion Energy (E_{torsion}), Total Energy (E_{total}), van der Waals Energy (E_{VDW}), etc), quantum chemistry parameters (i.e. Electronic Energy ($E_{\text{electronic}}$), HOMO Energy (E_{HOMO}) and LUMO Energy (E_{LUMO})), hydrophobic parameters (such as Clog P), stereo parameters (eg. Es, Balaban Index (BI), Connolly Accessible Area (CAA), Molecular Weight (MW), Shape Attribute (ShA), Total Connectivity (T_{con}), and Wiener Index (WI)), thermodynamic parameters, including Henry's Law Constant (H), Hydration Energy (E_{hyd}), Logarithm of partition coefficient in n-octanol/water (LogP), Molar Refractivity (MR), and molecular polar surface area (PSA). PSA is defined as the surface area (\AA^2) occupied by polar atoms, usually oxygen, nitrogen and hydrogen attached to them, which will restrict molecule penetration into the membranes (Chen et al, 2009). The other properties involved in number of hydrogen bond acceptor (NBA) and number of hydrogen bond donor (NBD).

The energy parameters root in the results of molecular mechanism and molecular dynamics. The total energy of a system expressed as follows (Iyer et al 2002):

$$E_{\text{total}} = E_{\text{valence}} + E_{\text{crossterm}} + E_{\text{nonbond}}$$

Here, the valence interactions includes bond stretching (bond), valence angle bending (angle), dihedral angle torsion (torsion), and inversion, also called out-of-plane interactions (oop) terms, which are part of nearly all forcefields for covalent systems. A Urey-Bradley term (UB) may be used to account for interactions between atom pairs involved in 1-3 configurations (i.e., atoms bound to a common atom): $E_{\text{valence}} = E_{\text{bond}} + E_{\text{angle}} + E_{\text{torsion}} + E_{\text{oop}} + E_{\text{UB}}$. Modern (second-generation) forcefields generally achieve higher accuracy by including cross terms to account for such factors as bond or angle distortions caused by nearby atoms. Crossterms can include the following terms: stretch-stretch, stretch-bend-stretch, bend-bend, torsion-stretch, torsion-bend-bend, bend-torsion-bend, stretch-torsion-stretch. The interaction energy between non-bonded atoms is accounted by van der Waals (VDW), electrostatic (Coulomb), and hydrogen bond (hbond) terms in some older forcefields. $E_{\text{non-bond}} = E_{\text{VDW}} + E_{\text{Coulomb}} + E_{\text{hbond}}$. Restraints that can be added to an energy expression include distance, angle, torsion, and inversion restraints. Restraints are useful if you, for example, are interested in only part of a structure for information on restraints and their implementation and use, and also the documentation for the particular simulation engine.

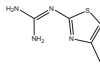
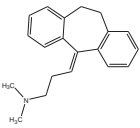
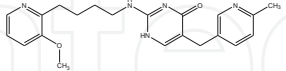

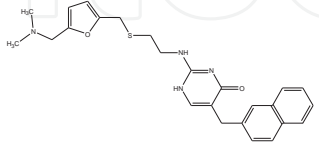
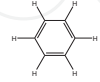
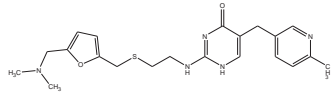
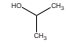
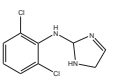
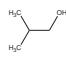
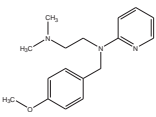
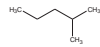
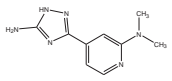
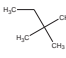
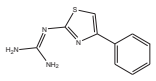
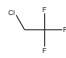
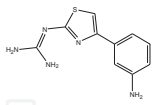
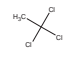
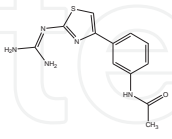
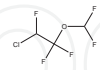
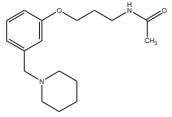
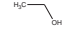
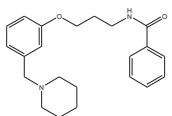
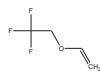
With the aid of Chemoffice Chem3D Ultra 8.0 and Hyperchem 7.5, we calculated the following descriptors by the procedure in detail below: (1) Draw the structures in ChemDraw 8.0; (2) Change structures to 3D by Chem3D; (3) Considering our chosen compounds, minimize the energy of the molecule based on molecular mechanism MM2 Force Field (Because under the MM2 force field, the time required for performing computations increases as N^2 , where N is the number of atoms.). We have chosen the job type as minimize energy to minimum RMS (root mean square) Gradient of 0.100 (the default value of 0.100 is a reasonable compromise between accuracy and speed). (4) Under the menu of Analyze-compute properties, select the properties to calculate and get every descriptor value of each compound.

QSAR models QSAR model of some purine derivatives (table 1) are achieved by partial sum of squares for regression with software SPSS 10.0. Some biological activity data are so large or small that the group of data cannot form a normal school, which is very important in lineal regression, and will surely degrade the accuracy of QSAR equations. So we discarded several data out of the normal school and some without necessary descriptors value. A training set of 26 structurally diverse purine derivatives are measured is used to construct QSAR models. The QSAR models are optimized using MLR fitting and stepwise method (Eq.1-Eq.5). A test set of five compounds is evaluated using the QSAR models as part of a validation process. Take MDR ratio in vitro in P388/VDR cell lines as dependent variable and molecule descriptors as independent variable. With the aid of Virtual Computational Chemistry Laboratory software (Wang et al, 2005), QSAR modeling was constructed by PLSR (Eq. 6).

Similarly, a training set of 18 structurally diverse propafenone analogs (table 2) are measured is used to construct QSAR models. The QSAR models are optimized using MLR fitting and stepwise method (Eq.7-Eq.11). Another QSAR modeling was constructed by PLSR (Eq. 12). A test set of five compounds is evaluated using the QSAR models as part of a validation process.

2.2. Blood-brain-barrier

Building of some compounds 37 organic compounds (Abraham et al, 1995; Abraham et al, 1997) were elected, composed a train set, and another 8 organic compounds were acted as a test set (table 3). The dependent variable used in this predictive model is the logarithm of the BBB partition coefficient, $\log BB = \log (C_{\text{brain}} / C_{\text{blood}})$, where C_{brain} is the concentration of the test compound in the brain, and C_{blood} is the concentration of the test compound in blood. Experimental values of $\log BB$ published to date lie approximately between -2.00 to +1.04. Compounds with $\log BB$ values of > 0.30 are readily distributed to the brain whereas compounds with values < -1.00 are poorly distributed to the brain. Building of all these compounds was performed on a PC computer using the Build modules of the commercial software packages Hyperchem 7.5. First, the geometry of these compounds was optimized using the Amber 94 force field in gas state. Second, they were placed at a periodic solvent box whose volume was $X=16\text{\AA}$, $Y=10\text{\AA}$, $Z=18\text{\AA}$, which included 96 water molecules. Here, temperature is 300°K and pressure is 1 standard atmosphere. Then, the compounds in water were minimized by the above method. Third, the compounds in water were simulated by Monte Carlo method and minimized by the above method.

No	Structure	LogBB	No	Structure	LogBB
Training set					
B1		-0.04	B20		0.85
B2		-2.00	B21		0.03
B3		-1.30	B22		0.37
B4		-1.06	B23		-0.15
B5		0.11	B24		-0.17
B6		0.49	B25		0.97
B7		-1.17	B26		1.04
B8		-0.18	B27		0.08
B9		-1.15	B28		0.40
B10		-1.57	B29		0.24
B11		-0.46	B30		-0.16
B12		-0.24	B31		0.13

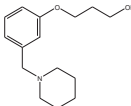
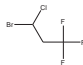
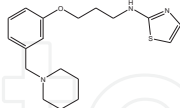
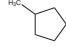
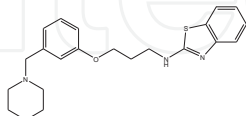
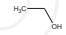
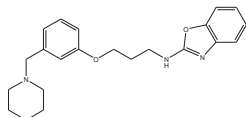
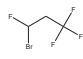
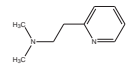
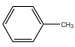
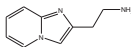
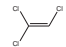
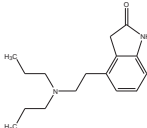
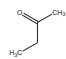
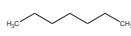
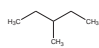

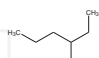
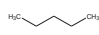
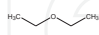
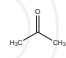
No	Structure	LogBB	No	Structure	LogBB
B13		-0.02	B32		0.35
B14		0.44	B33		0.93
B15		0.14	B34		-0.16
B16		0.22	B35		0.27
B17		-0.06	B36		0.37
B18		-1.40	B37		0.34
B19		0.25			
Test set					
T1		-0.08	T5		0.81
T2		1.01	T6		0.04
T3		0.90	T7		0.76
T4		0.00	T8		-0.15

Table 3. The structures and LogBB values of some compounds in the training/test sets.

Molecular modeling of a DMPC monolayer membrane complex with a layer of water. A model of dimyristoylphosphatidylcholine (DMPC) monolayer membrane was constructed using the software Material Studio, and minimized for 200 steps with the smart minimizer. The DMPC monolayer membrane was composed of 25 DMPC molecules ($5 \times 5 \times 1$). Here, the parameter of the single crystal of DMPC was $a=8\text{\AA}$, $b=8\text{\AA}$, and $\gamma=96.0$, which resulted average area of each lipid molecule 64\AA^2 similar to Stouch's research results (Bassolino-Klimas et al, 1993). Moreover, we add a layer of water ($40 \times 40 \times 10$) including 529 water molecules to the

polar side of the DMPC monolayer membrane. Figure 1 showed the dominant conformation of B1 compound colored by atom-type in water. The red box denotes the water solvent box defined in Monte Carlo simulation.

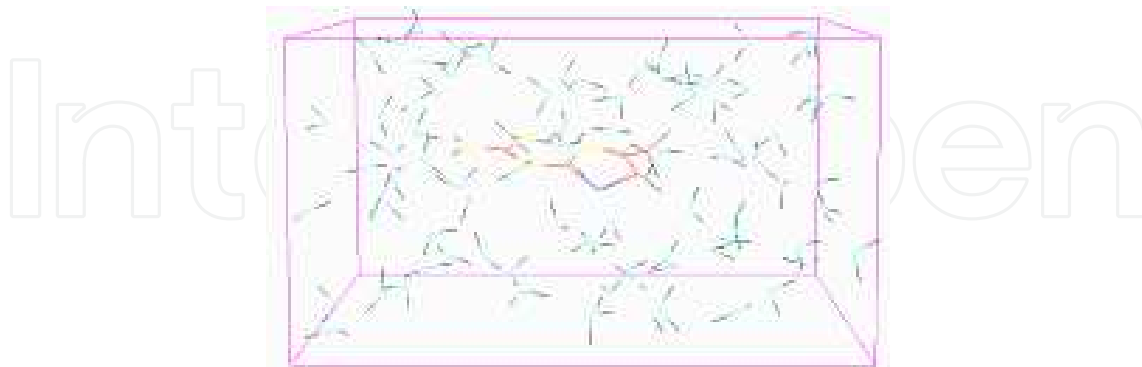


Figure 1. The dominant conformation of B1 compound colored by atom-type in water. The red box denotes the water solvent box defined in Monte Carlo simulation.

Molecular dynamic simulation of a small molecule complex with DMPC-water model. A DMPC molecule at the center of the above DMPC monolayer membrane complex with a layer of water was replaced with an organic compound to form a solute-membrane-water complex. The center organic compound was inserted at three different positions in the DMPC-water model before the start of each of the three corresponding molecular dynamics simulation. Molecular dynamic simulation of the complex was performed for 1000 steps by Discover module with Materials Studios, using Compass force field. Here, the three-dimensional volume was restricted to a border of $X=40\text{\AA}$, $Y=40\text{\AA}$, $Z=91.76\text{\AA}$, and $\gamma=96.0$.

QSAR model of BBB partitioning of some compounds. MI-QSAR model of some organic compounds through BBB are achieved by partial sum of squares for regression with software SPSS. A training set of 37 structurally diverse compounds whose BBB partition coefficients are measured is used to construct QSAR models. Molecular dynamics simulations are used to determine the explicit interaction of each test compound with a model of DMPC monolayer membrane complex with a layer of water. An additional set of intramolecular solute descriptors are computed and considered in the trial pool of descriptors for building MI-QSAR models. The QSAR models are optimized using multidimensional linear regression fitting and stepwise method. A test set of eight compounds is evaluated using the MI-QSAR models as part of a validation process.

3. Results

3.1. QSAR analysis based on MDR ratio in P388/VDR-20 and KB-A1 in vitro

Take MDR ratio in vitro in KB-A1/ADR cell lines as dependent variable and molecule descriptors as independent variable. A training set of 26 structurally diverse compounds (Table 4) was

used to construct QSAR models. The QSAR models were optimized using MLR fitting and stepwise method by the SPSS software (Eq.1-Eq.5). A test set of 5 compounds (compound A27-A31) was evaluated using the models as part of a validation process (figure 2 upper, Table 5).

Meanwhile, take MDR ratio in vitro in P388/VDR cell lines as dependent variable and molecule descriptors as independent variable. With the aid of Virtual Computational Chemistry Laboratory software (<http://vcclab.org>) (Wang et al, 2005), construct QSAR modeling by PLSR (Eq.6, figure 2 down). Table 6 shows the calculated descriptors mentioned above and the result of predicted value was in Table 5.

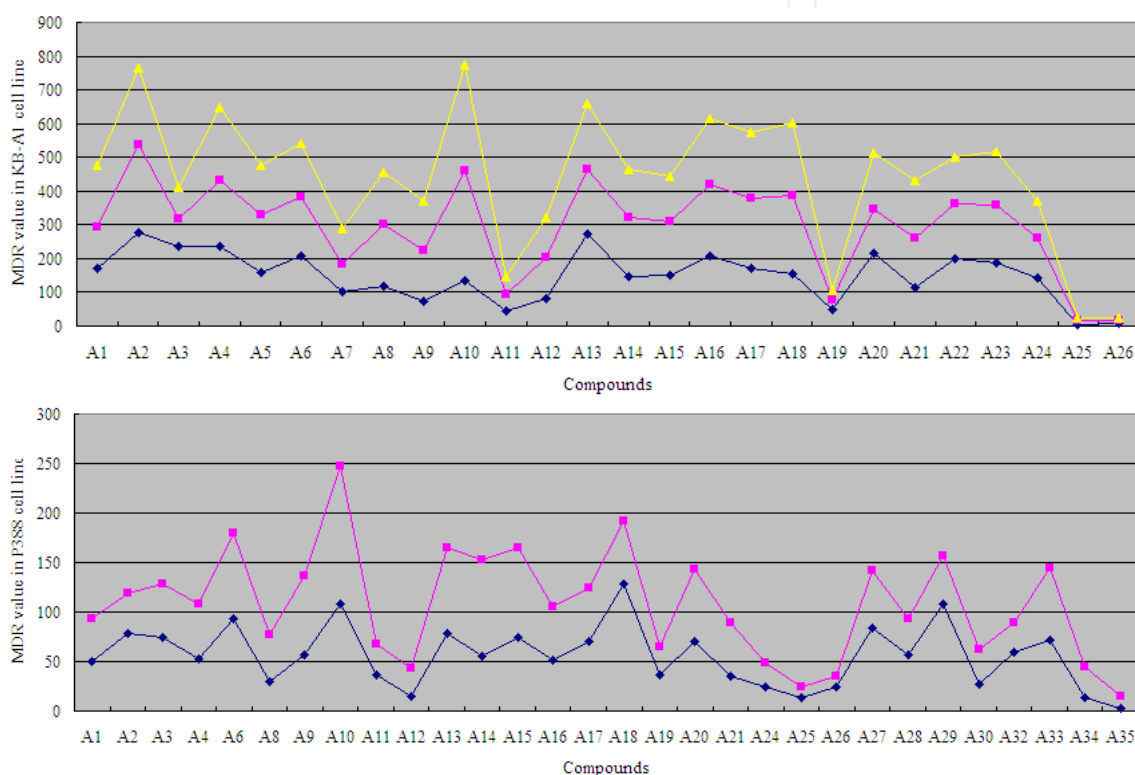


Figure 2. Comparison of the experimental MDR values with the corresponding predicted MDR values. Upper: MDR value in KB-A1/ADR cell lines (blue rhombic dots); MDR as predicted by Eq.4 MLR model (red square dots) and by Eq.5 MLR model (yellow triangle dots) for all the molecules of the training and test set. Down: MDR value in P388/VDR cell lines (blue rhombic dots); MDR as predicted by the method of PLSR (Eq. 6) (red square dots) for all the molecules of the training and test set. The rhombic dots represented the experimental values (P388) and the predicted values of MDR, respectively.

$$\begin{aligned} \text{LogMDR} &= -6.537 + 7.162\text{LogMR} \\ \text{N} &= 27; \text{R} = 0.445; \text{F} = 6.187 \end{aligned} \quad (1)$$

$$\begin{aligned} \text{LogMDR} &= -37.830 + 48.862\text{LogMR} - 0.499\text{ShA} \\ \text{N} &= 27; \text{R} = 0.889; \text{F} = 45.415 \end{aligned} \quad (2)$$

$$\text{LogMDR} = -35.816 + 52.416\text{LogMR} - 0.717 \times \text{ShA} + 6.612 \times 10^{-7} \text{BI}$$

$$\text{N} = 27; \text{R} = 0.919; \text{F} = 41.442 \quad (3)$$

$$\text{LogMDR} = -38.791 + 56.923\text{LogMR} - 0.769\text{ShA} + 5.897 \times 10^{-7} \text{BI} - 0.159\text{LogP}$$

$$\text{N} = 27; \text{R} = 0.927; \text{F} = 33.504 \quad (4)$$

$$\text{LogMDR} = -42.192 + 61.818\text{LogMR} -$$

$$-0.801\text{ShA} + 4.791 \times 10^{-7} \text{BI} - 0.369\text{LogP} + 3.595 \times 10^{-2} E_{\text{hyd}}$$

$$\text{N} = 27; \text{R} = 0.936; \text{F} = 29.749 \quad (5)$$

$$\text{LogMDR} = 7.611 + 3.138 \times 10^{-2} \text{LogP} - 0.245\text{MR} + 0.495 E_{\text{VDW}} - 0.509\text{ShA} + 8.802 \times 10^{-4} \text{WI}$$

$$\text{N} = 30; \text{Q}^2 = 0.4650 \quad (6)$$

No.	Log MR	ShA	BI	LogP	E_{hyd} (kcal/mol)	No.	Log MR	ShA	BI	LogP	E_{hyd} (kcal/mol)
Training set											
A1	1.20	37.03	2662570	3.33	-3.56	A14	1.22	39.02	3358755	1.48	-19.64
A2	1.18	35.03	2440928	2.59	-13.71	A15	1.22	39.02	3358755	1.48	-19.71
A3	1.22	40.02	3649082	1.14	-16.23	A16	1.20	37.03	2662570	2.13	-15.99
A4	1.14	32.03	1669953	2.21	-13.54	A17	1.202	37.03	2662570	2.13	-16.23
A5	1.22	39.02	3358755	1.33	-19.71	A18	1.202	37.03	2662570	2.13	-15.95
A6	1.20	37.03	2662570	2.13	-16.22	A19	1.18	37.03	3091919	1.61	-15.9
A7	1.22	40.02	3491392	0.76	-17.67	A20	1.23	41.02	4008723	0.76	-17.36
A8	1.20	37.03	2662570	2.28	-16.3	A21	1.14	32.03	1651352	1.9	-13.79
A9	1.24	42.02	4491514	1.29	-16.34	A22	1.22	39.02	3324212	1.33	-20.06
A10	1.24	41.02	4055919	0.99	-19.77	A23	1.20	37.03	2634052	2.13	-15.77
A11	1.18	36.03	2271976	1.41	-17.73	A24	1.19	36.03	2246188	2.13	-16.15
A12	1.19	36.03	2271976	2.13	-16.17	A25	1.15	35.03	2244801	1.71	-14.88
A13	1.15	33.03	1900460	2.28	-13.57	A26	1.15	35.03	2271261	1.71	-15.03
Test set											
A27	1.19	37.03	2662570	1.41	-18.09	A30	1.25	41.02	3977672	2.98	-13.52
A28	1.22	40.02	3491392	0.76	-17.61	A31	1.20	37.03	2634052	2.13	-15.95
A29	1.21	37.03	2662570	2.75	-15.55						

Table 4. The molecular descriptors of some compounds related to MDR ratios in the training/test sets

No.	MDR ratio (KB- A1)	Predictive values of MDR ratio					No.	MDR ratio (KB- A1)	Predictive values of MDR ratio				
		Eq.1	Eq.2	Eq.3	Eq.4	Eq.5			Eq.1	Eq.2	Eq.3	Eq.4	Eq.5
Training set													
A1	171	114.32	215.61	200.33	123.15	180.87	A14	147	151.94	151.04	171.02	173.75	144.79
A2	278	80.79	200.54	305.22	260.52	228.39	A15	152	150.27	140.09	157.75	159.16	130.87
A3	238	161.08	71.37	78.37	79.12	92.55	A16	209	115.64	233.15	217.87	209.32	197.83
A4	236	44.84	113.11	178.94	196.99	213.61	A17	171	115.64	233.15	217.87	209.32	193.94
A5	160	150.27	140.09	157.75	168.14	148.66	A18	156	116.97	252.09	236.91	229.26	219.10
A6	208	113.02	199.36	184.18	174.42	159.21	A19	49	81.98	22.31	33.79	29.47	25.56
A7	102	163.01	77.39	67.24	80.67	105.63	A20	214	198.44	93.91	119.73	132.46	165.76
A8	120	114.32	215.61	200.33	180.88	153.75	A21	113	42.69	80.90	121.41	145.60	174.56
A9	75	237.62	101.82	179.28	149.94	146.81	A22	200	150.27	140.09	149.67	160.44	139.02
A10	136	222.49	204.96	297.19	322.30	315.82	A23	189	113.02	199.36	176.36	167.80	160.14
A11	44	79.86	58.80	41.66	49.61	53.08	A24	142	92.42	159.30	116.68	117.52	112.54
A12	83	92.42	159.30	121.35	121.70	115.60	A25	6	52.12	10.08	9.16	8.45	8.02
A13	272	53.80	124.41	185.32	190.50	197.66	A26	9	52.12	10.08	9.53	8.76	8.16
Testset													
A27	406	99.21	81.97	70.98	80.61	81.67	A30	370	243.10	375.08	504.47	282.78	192.47
A28	68	163.01	77.39	67.24	80.67	106.16	A31	210	114.32	215.61	191.82	183.83	174.21
A29	723	125.69	411.51	400.76	323.36	248.59							

Table 5. The experimental values and the predictive values of MDR ratio of these compounds.

No.	MDR (P388)	Pred MDR	LogP	MR	E _{VDW}	ShA	WI	No.	MDR (P388)	Pred MDR	LogP	MR	E _{VDW}	ShA	WI
A1	50	43.66	3.33	15.85	32.21	37.03	5476	A18	129	62.87	2.13	15.90	27.08	37.03	5476
A2	78	40.71	2.59	15.10	21.84	35.08	4872	A19	36	29.48	1.61	15.13	21.63	37.03	5585
A3	75	53.15	1.14	16.63	24.83	40.02	6522	A20	70	73.87	0.76	17.12	25.52	41.02	6855
A4	53	55.39	2.21	13.91	20.16	32.03	3916	A21	35	54.41	1.9	13.82	20.17	32.03	3874
A6	93	86.84	2.13	15.83	32.75	37.03	5476	A24	24	24.57	2.13	15.39	23.42	36.03	4855
A8	30	47.64	2.28	15.85	25.21	37.03	5476	A25	13	11.32	1.71	14.21	22.20	35.03	4487
A9	57	79.51	1.29	17.56	26.03	42.02	7353	A26	24	11.44	1.71	14.21	20.92	35.03	4538
A10	108	138.69	0.99	17.40	29.44	41.02	6935	A27	84	58.01	1.41	15.54	26.05	37.03	5476

No.	MDR	Pred	LogP	MR	E _{VDW}	ShA	WI	No.	MDR	Pred	LogP	MR	E _{VDW}	ShA	WI
	(P388)	MDR						(P388)	MDR						
A11	37	30.21	1.41	15.08	24.04	36.03	4909	A28	57	35.88	0.76	16.66	23.78	40.02	6244
A12	15	27.61	2.13	15.39	23.512	36.03	4909	A29	108	49.03	2.75	16.06	25.95	37.03	5476
A13	78	87.23	2.28	14.27	29.12	33.03	4216	A30	27	35.79	2.98	17.61	26.49	41.02	6804
A14	56	96.24	1.48	16.50	28.19	39.02	6288	A32	59	30.18	1.83	15.13	22.08	37.03	5642
A15	75	89.20	1.48	16.47	27.54	39.02	6288	A33	71	73.84	0.86	15.79	27.62	38.03	5822
A16	51	54.90	2.13	15.88	25.61	37.03	5476	A34	13	31.95	2.58	15.64	25.36	37.03	5476
A17	70	54.43	2.13	15.88	25.49	37.03	5476	A35	3	12.22	1.71	14.21	20.40	35.03	4589

Table 6. Comparison of experimental value of MDR ratio with predicted value of MDR ratio by PLSR.

3.2. QSAR analysis based on Ka of ATPase in CCRF ADR5000 cell lines

Similarly, take Ka of ATPase in CCRF ADR5000 cell lines as dependent variable and molecule descriptors as independent variable. We construct QSAR models using two methods, MLD method (Eq.7-Eq.11) and PLSR method (Eq.12) (see figure 3).

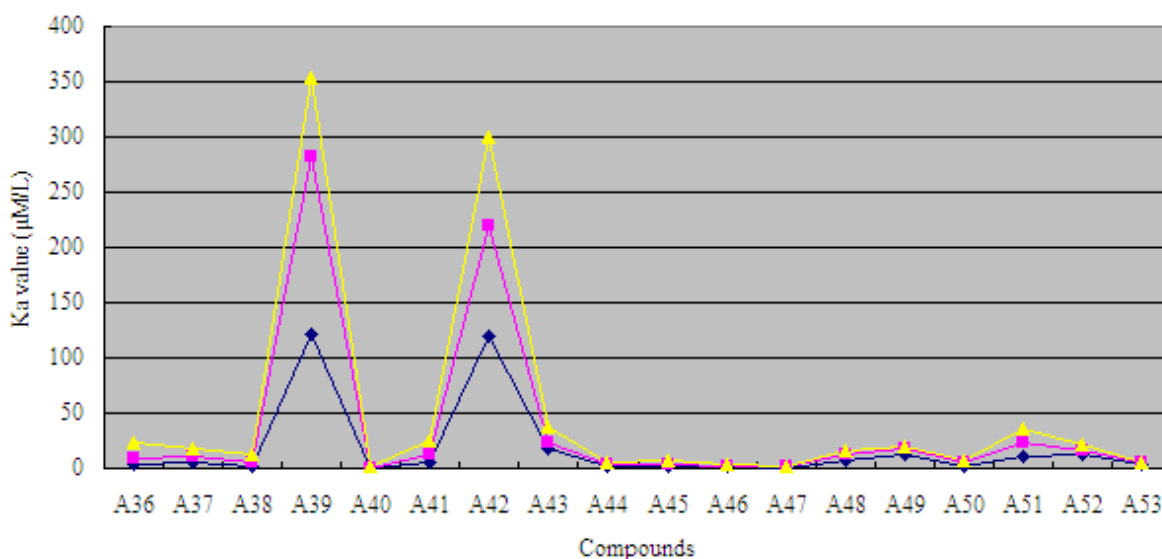


Figure 3. Comparison of the experimental Ka value (blue rhombic dots) with the corresponding predicted Ka as predicted by Eq.11 MLR model (red square dots) and by Eq.12 PLSR model (yellow triangle dots) for all the molecules of the training and test.

A training set of 16 structurally diverse compounds was used to construct QSAR models. All the molecular descriptors were calculated as Table 7. The QSAR models were optimized using MLR fitting and stepwise method. A test set of 2 compounds was evaluated using the models as part of a validation process. Table 8 displays the comparison of the experiment and prediction value.

$$\text{LogKa} = 2.424 - 0.484\text{LogP}$$

N= 16; R= 0.860; F=39.748 (7)

$$\text{LogKa} = 3.612 - 0.285\text{LogP} - 0.0732\text{ShA}$$

N= 16; R= 0.900; F=27.676 (8)

$$\text{LogKa} = 2.573 - 0.480\text{LogP} - 0.285\text{ShA} + 0.651\text{MR}$$

N= 16; R= 0.914; F=20.251 (9)

$$\text{LogKa} = 7.313 - 0.752\text{LogP} - 0.647\text{ShA} + 1.642\text{MR} + 0.605E_{\text{HOMO}}$$

N= 16; R= 0.928; F=17.111 (10)

$$\text{LogKa} = 10.021 - 0.875\text{LogP} - 1.044\text{ShA} + 2.263\text{MR} + 0.673E_{\text{HOMO}} + 6.734 \times 10^{-4}\text{WI}$$

N= 16; R=0.945; F=16.832 (11)

$$\text{LogKa} = 3.662 - 0.279\text{LogP} - 4.71 \times 10^{-3}\text{MW} + 1.223 \times 10^{-2}E_{\text{HOMO}}$$

N=18, Q²=0.7100 (12)

No.	LogP	ShA	MR	E _{HOMO} (eV)	WI	MW	No.	LogP	ShA	MR	E _{HOMO} (eV)	WI	MW
A36	3.39	21.04	9.254	-9.14	1366	312.41	A45	4.3	26.04	11.42	-9.17	2345	383.53
A37	3.62	24.04	10.55	-9.20	1949	355.48	A46	4.93	32.03	13.27	-8.24	4689	462.57
A38	3.67	25.04	10.84	-9.16	2172	367.49	A47	5.2	32.03	13.38	-8.19	4329	464.58
A39	1.42	18.05	7.86	-9.12	920	277.37	A48	4.25	26.04	11.45	-9.24	2607	383.53
A40	4.93	32.03	13.27	-8.16	4329	462.57	A49	4.52	26.04	11.59	-8.94	2367	385.55
A41	2.67	25.04	10.29	-8.15	2244	372.44	A50	4.88	27.03	12.06	-8.94	2550	399.58
A42	0.94	19.05	8.01	-9.15	1050	293.37	A51	2.38	26.04	10.99	-9.09	2400	383.49
A43	2.54	25.04	10.52	-9.20	2172	369.46	A52	3.94	25.04	10.95	-9.05	2172	369.51
A44	3.98	32.03	13.50	-9.16	4227	459.59	A53	4.93	32.03	13.27	-8.19	4509	462.57

Table 7. The molecular descriptors of some compounds related to ATPase in the training/test sets.

No.	Ka ($\mu\text{M/L}$)	Predictive values of Ka						No.	Ka ($\mu\text{M/L}$)	Predictive values of Ka					
		Eg.7	Eg.8	Eg.9	Eg.10	Eg.11	Eg.12			Eg.7	Eg.8	Eg.9	Eg.10	Eg.11	Eg.12
A36	3.34	6.07	12.75	9.37	6.43	6.14	13.57	A45	1.53	2.20	3.02	3.32	2.69	2.08	3.50
A37	5.30	4.70	6.62	7.10	6.19	5.60	7.33	A46	1.47	1.09	0.73	0.52	0.48	0.81	1.02
A38	2.59	4.44	5.41	5.36	3.98	3.06	6.24	A47	0.55	0.81	0.61	0.46	0.50	0.53	0.84
A39	122	54.54	76.92	73.09	90.64	160.46	70.37	A48	7.64	2.33	3.13	3.83	3.33	4.22	3.60
A40	0.36	1.09	0.73	0.52	0.53	0.51	1.02	A49	12.20	1.72	2.62	3.39	4.98	5.00	2.99
A41	6.13	13.54	10.43	7.17	11.79	7.23	11.56	A50	2.26	1.15	1.75	2.37	3.50	3.28	2.04
A42	120.00	93.12	89.09	81.21	80.47	99.37	80.44	A51	10.50	18.71	10.66	14.57	16.6	13.20	12.02
A43	18.50	15.65	11.36	11.73	8.26	5.56	12.59	A52	12.80	3.29	4.53	4.74	4.57	3.91	5.15
A44	1.01	3.15	1.36	2.10	1.66	2.13	1.88	A53	4.15	1.09	0.73	0.52	0.51	0.65	1.02

Table 8. Comparison the experimental values with the predictive values of Ka of these compounds.

3.3. QSAR analysis based on blood-brain barrier partitioning of organic compounds

37 organic compounds of training set and 8 compounds of test set are built and minimized, dissolved in liquid, and are optimized by Monte Carlo method and molecular mechanism, finally the dominant conformation of these compounds are obtained. Molecular modeling of a small molecule complex with the membrane-water model reveals that the energy of an organic compound inserted at the middle position in the DMPC model with a layer of water is lower than that of the other two positions. MI-QSAR analysis has been used to develop predictive models of some organic compounds through BBB, in part, simulating the interaction of an organic compound with the phospholipide-rich regions of cellular membranes surrounding by a layer of water. Molecular descriptors of compounds in a training set and a test set are listed in Table 9. Six QSAR equations were constructed based on Table 9 and were listed as follows.

$$\log BB = 0.552 - 1.73 \times 10^{-2} PSA$$

$$n = 37 \quad R = 0.835 \quad S = 0.398 \quad (13)$$

$$\log BB = 0.229 - 1.70 \times 10^{-2} PSA + 0.131C \log P$$

$$n = 37 \quad R = 0.878 \quad S = 0.352 \quad (14)$$

$$\log BB = 4.965 \times 10^{-2} - 1.28 \times 10^{-2} PSA + 0.211C \log P - 6.40 \times 10^{-7} BI$$

$$n = 37 \quad R = 0.924 \quad S = 0.285 \quad (15)$$

$$\log BB = 6.262 \times 10^{-2} - 1.36 \times 10^{-2} PSA + 0.205 C \log P - 7.11 \times 10^{-7} BI - 0.185 E_{stretch}$$

$$n = 37 \quad R = 0.938 \quad S = 0.264 \quad (16)$$

$$\log BB = 6.580 \times 10^{-2} - 1.21 \times 10^{-2} PSA + 0.206 C \log P - 7.77 \times 10^{-7} BI - 0.197 E_{stretch} +$$

$$+ 1.330 \times 10^{-3} \Delta E_{total}$$

$$n = 37 \quad R = 0.947 \quad S = 0.248 \quad (17)$$

$$\log BB = 8.730 \times 10^{-2} - 1.04 \times 10^{-2} PSA + 0.222 C \log P - 9.60 \times 10^{-7} BI - 0.183 E_{stretch} +$$

$$+ 1.364 \times 10^{-3} \Delta E_{total} - 2.68 \times 10^{-3} \Delta E_{torsion}$$

$$n = 37 \quad R = 0.955 \quad S^2 = 0.232 \quad (18)$$

Here, n means the number of compounds in a training set, R means the correlative coefficient, and S means the standard residual error. $\log BB = \log (C_{brain}/C_{blood})$. PSA means the total polar surface area of a molecule. $C \log P$ and BI display calculated $\log P$ and connective index of molecular average total distance (relative covalent radius), respectively. They come from CS calculation. ΔE_{total} and $\Delta E_{torsion}$ are related to interaction between an organic compound and membrane-water model. The total energy and the torsion energy of the DMPC monolayer membrane complex with a layer of water are -340.7589 and -1724.4164 (Kcal/mol), respectively. ΔE_{total} is the change in the total potential energy of the solute-membrane-water complex comparing with that of the membrane-water model and so is $\Delta E_{torsion}$.

No	PSA (Å ²)	ClogP	BI(Å)	$E_{stretch}$ (Kcal/mol)	E_{total}^a (Kcal/mol)	$E_{torsion}^a$ (Kcal/mol)	ΔE_{total}^b (Kcal/mol)	$\Delta E_{torsion}^b$ (Kcal/mol)
Training set								
B1	78.90	1.20	12378	-1.35503	-298.2972	-1713.1146	42.46	11.30
B2	94.00	1.99	1101758	-0.15595	-406.0803	-1789.8084	-65.32	-65.39
B3	73.00	3.80	1738650	-1.48472	-256.3021	-1703.1425	84.46	21.27
B4	87.00	1.63	1346396	-1.39112	-302.7543	-1841.5635	38.00	-117.15
B5	39.00	1.02	41807	0.58131	-226.3773	-1734.7452	114.38	-10.33
B6	26.80	3.23	305770	-0.09264	-228.2923	-1679.4604	112.47	44.96
B7	88.80	1.01	58510	0.71038	-279.0781	-1671.3414	61.68	53.07
B8	76.60	2.80	62216	-0.38334	-309.2981	-1654.6730	31.46	69.74

No	PSA (Å ²)	ClogP	BI(Å)	E _{stretch} (Kcal/mol)	E _{total} ^a (Kcal/mol)	E _{torsion} ^a (Kcal/mol)	ΔE _{total} ^b (Kcal/mol)	ΔE _{torsion} ^b (Kcal/mol)
Training set								
B9	104.40	1.77	83798	-0.35599	-313.4237	-1639.9898	27.34	84.43
B10	108.80	2.00	193593	-0.52172	-548.5593	-1640.9214	-207.80	83.49
B11	47.90	2.51	352512	-0.09496	-312.1226	-1656.7465	28.64	67.67
B12	45.20	4.27	779210	0.00479	-163.8011	-1716.3101	176.96	8.11
B13	38.50	2.61	158640	-0.09491	-170.3338	-1716.7159	170.43	7.70
B14	40.00	4.28	431722	-1.30506	-247.0951	-1748.0241	93.66	-23.61
B15	39.20	5.88	766256	0.09911	-289.2825	-1735.4004	51.48	-10.98
B16	54.90	5.14	766256	-0.14215	-181.0636	-1743.6068	159.70	-19.19
B17	18.80	0.62	20863	0.18071	-331.7044	-1695.6999	9.05	28.72
B18	46.70	0.27	20264	-1.36843	-209.4697	-1644.6752	131.29	79.74
B19	44.10	2.80	190375	-2.97778	-311.9182	-1713.8942	28.84	10.52
B20	5.40	4.85	210631	-0.06079	-235.7250	-1704.3399	105.03	20.08
B21	0.00	-0.47	4	0.00000	-407.3194	-1729.3793	-66.56	-4.96
B22	0.00	2.14	972	-0.00009	-239.8807	-1675.1827	100.88	49.23
B23	23.40	0.07	213	0.00000	-160.1278	-1672.3898	180.63	52.03
B24	22.60	0.69	712	0.00000	-319.0674	-1742.6968	21.69	-18.28
B25	0.00	3.74	1899	0.00067	-282.3721	-1751.6193	58.39	-27.20
B26	0.00	3.61	1661	0.00000	-285.7132	-1731.9518	55.05	-7.54
B27	0.00	1.43	1661	-0.00008	-238.7249	-1731.3090	102.03	-6.89
B28	0.00	2.48	633	0.00003	-291.5583	-1725.7370	49.20	-1.32
B29	11.60	2.46	21380	-0.00005	-418.0323	-1682.7138	-77.27	41.70
B30	24.40	-0.24	47	0.00000	-329.3150	-1704.6187	11.44	19.80
B31	10.70	1.27	7864	-0.00002	-253.3453	-1747.7044	87.41	-23.29
B32	0.00	2.37	7322	-0.00003	-268.8335	-1714.2486	71.93	10.17
B33	0.00	3.31	931	0.02567	-353.8395	-1739.7672	-13.08	-15.35
B34	24.40	-0.24	47	0.00000	-187.4520	-1720.5500	153.31	3.87
B35	0.00	1.93	7322	-0.00003	-177.4875	-1728.8621	163.27	-4.45

No	PSA (\AA^2)	ClogP	BI(\AA)	E_{stretch} (Kcal/mol)	E_{total}^a (Kcal/mol)	E_{torsion}^a (Kcal/mol)	$\Delta E_{\text{total}}^b$ (Kcal/mol)	$\Delta E_{\text{torsion}}^b$ (Kcal/mol)
Training set								
B36	0.00	2.64	2050	-0.02344	-220.3940	-1681.1548	120.36	43.26
B37	0.00	2.63	712	-0.00002	-231.5752	-1722.2582	109.18	2.16
Test set								
T1	22.70	0.321	712	0.00000	-274.7201	-1713.7409	66.04	10.68
T2	0.00	3.738	1838	0.00000	-225.6308	-1716.6234	115.13	7.79
T3	0.00	4.267	4150	0.00000	-331.3754	-1700.6397	9.38	23.78
T4	11.30	0.870	791	0.00000	-181.5954	-1700.8447	159.16	23.57
T5	0.00	4.397	4650	0.00000	-404.2903	-1741.2420	-63.53	-16.83
T6	0.00	1.103	0	0.00000	-282.9386	-1746.1889	57.82	-21.77
T7	0.00	3.339	791	0.00063	-271.9174	-1681.9440	68.84	42.47
T8	22.70	-0.208	213	0.00000	-364.8884	-1695.3605	-24.13	29.06

Note: ^a E_{total} and E_{torsion} mean the total energy and the torsion energy of the complex with an organic compound and DMPC monolayer membrane. ^b The total energy and the torsion energy of the DMPC monolayer membrane are -340.758901 and -1724.416387 (Kcal/mol). ΔE_{total} and $\Delta E_{\text{torsion}}$ are the residues between a complex of an organic compound with DMPC monolayer membrane and the DMPC monolayer membrane.

Table 9. The molecular descriptors of the compounds related to BBB in the training/test sets

With the increase of the variable from one to six, the relativity of QSAR equation is also improved, and the predictive ability of the model is enhanced. Eq.18 is most significant, which means that the capability of an organic compound through BBB depends upon PSA, ClogP, BI, E_{stretch} , ΔE_{total} , and $\Delta E_{\text{torsion}}$. Moreover, the potential of an organic compound through BBB is directly proportional to ClogP and ΔE_{total} , but inversely proportional to PSA, BI, E_{stretch} , and $\Delta E_{\text{torsion}}$. The observed and predicted log BB values of the training set compounds are listed in Table 10. Figure 4 shows the comparison of the experimental log BB values for all the molecules of the training set with the corresponding predicted log BB as predicted by Eq.17 and -18 MI-QSAR models. Compound B18 in the training set is predicted to have a much higher log BB than observed, and this molecule has also been identified as an outlier in other studies (Iyer et al, 2002). Protonation of the molecule could account for its low log BB value.

A test set of eight solute compounds was constructed as one way to attempt to validate the QSAR models given by six equations mentioned. The test set compounds were selected so as to span almost the entire range in BBB partitioning. The observed and predicted log BB values for this test set are given in Table 10 and plotted in Figure 4 (right). It seems to suggest that Eq. 17 and -18 QSAR models could predict log BB for other compounds in drug design.

No	LogBB	Predictive Value of logBB						No	LogBB	Predictive Value of logBB					
		Eg.13	Eg.14	Eg.15	Eg.16	Eg.17	Eg.18			Eg.13	Eg.14	Eg.15	Eg.16	Eg.17	Eg.18
Training set															
B1	-0.04	-0.81	-0.95	-0.71	-0.52	-0.33	-0.20	B20	0.85	0.46	0.77	0.87	0.85	0.99	1.01
B2	-2.00	-1.07	-1.11	-1.44	-1.56	-1.57	-1.39	B21	0.03	0.55	0.17	-0.05	-0.03	-0.12	-0.10
B3	-1.30	-0.71	-0.51	-1.20	-1.11	-0.98	-1.17	B22	0.37	0.55	0.51	0.50	0.50	0.64	0.57
B4	-1.06	-0.95	-1.04	-1.58	-1.49	-1.37	-1.13	B23	-0.15	0.15	-0.16	-0.23	-0.24	0.04	-0.03
B5	0.11	-0.12	-0.30	-0.26	-0.40	-0.19	-0.06	B24	-0.17	0.16	-0.06	-0.09	-0.10	-0.04	0.08
B6	0.49	0.09	0.20	0.19	0.16	0.34	0.28	B25	0.97	0.55	0.72	0.84	0.83	0.91	1.07
B7	-1.17	-0.98	-1.15	-0.91	-1.11	-0.90	-0.86	B26	1.04	0.55	0.70	0.81	0.80	0.88	0.98
B8	-0.18	-0.77	-0.71	-0.38	-0.38	-0.22	-0.22	B27	0.08	0.55	0.42	0.35	0.35	0.49	0.56
B9	-1.15	-1.25	-1.31	-0.97	-0.99	-0.79	-0.81	B28	0.40	0.55	0.55	0.57	0.57	0.64	0.71
B10	-1.57	-1.33	-1.36	-1.05	-1.05	-1.16	-1.20	B29	0.24	0.35	0.35	0.41	0.39	0.31	0.27
B11	-0.46	-0.28	-0.26	-0.26	-0.31	-0.21	-0.32	B30	-0.16	0.13	-0.22	-0.31	-0.32	-0.26	-0.26
B12	-0.24	-0.23	0.02	-0.13	-0.23	0.03	0.04	B31	0.13	0.37	0.21	0.18	0.17	0.31	0.43
B13	-0.02	-0.11	-0.08	0.01	-0.02	0.26	0.34	B32	0.35	0.55	0.54	0.55	0.54	0.64	0.68
B14	0.44	-0.14	0.11	0.17	0.33	0.51	0.64	B33	0.93	0.55	0.66	0.75	0.74	0.73	0.84
B15	0.14	-0.13	0.33	0.30	0.17	0.26	0.33	B34	-0.16	0.13	-0.22	-0.31	-0.32	-0.07	-0.02
B16	0.22	-0.40	-0.03	-0.06	-0.15	0.10	0.22	B35	0.27	0.55	0.48	0.45	0.45	0.68	0.74
B17	-0.06	0.23	-0.01	-0.07	-0.11	-0.07	-0.09	B36	0.37	0.55	0.57	0.61	0.61	0.77	0.72
B18	-1.40	-0.26	-0.53	-0.50	-0.28	-0.02	-0.14	B37	0.34	0.55	0.57	0.60	0.60	0.75	0.81
B19	0.25	-0.21	-0.15	-0.05	0.45	0.59	0.62								
Test set															
T1	-0.08	0.16	-0.11	-0.17	-0.18	-0.06	-0.02	T5	0.81	0.55	0.81	0.97	0.96	0.88	1.02
T2	1.01	0.55	0.72	0.84	0.83	0.99	1.05	T6	0.04	0.55	0.37	0.28	0.29	0.37	0.47
T3	0.90	0.55	0.79	0.95	0.93	0.95	0.98	T7	0.76	0.55	0.67	0.75	0.75	0.84	0.81
T4	0.00	0.36	0.15	0.09	0.09	0.32	0.32	T8	-0.15	0.16	-0.18	-0.28	-0.29	-0.28	-0.31

Table 10. The experimental values and the predictive values of LogBB of these compounds.

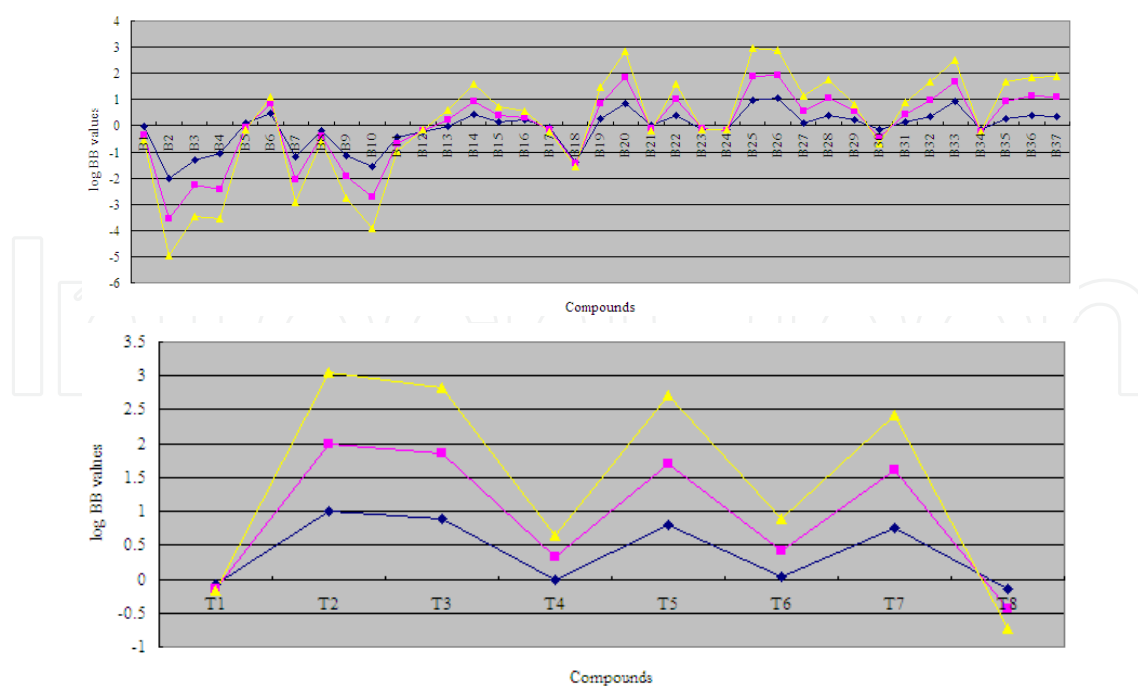


Figure 4. Comparison of the experimental log BB values (blue rhombic dots) for all the molecules of the training sets (upper) or the test set (down) to the corresponding predicted log BB as predicted by Eg.17 MI-QSAR model (red square dots) and by Eg.18 MI-QSAR model (yellow triangle dots).

4. Discussion

We have built some predictive models of MDR, K_a and BBB partitioning of organic compounds by simulating the interaction of modulators or drugs interact with P-gp and/or of an organic compound with the phospholipide-rich regions of cellular membranes. As we know in the introduction part, modulators or drugs interact with P-gp and thus reduce the efflux of the cytotoxic compounds will increase the apparent toxicity of the cytotoxic compounds. It is very important to keep in mind that it is based on a general assessment of cytotoxicity and thus may account for more than one acting mechanism in the resistant cells used. So there are many uncertainty factors in the MDR ratio assay method and it is also convinced by our linear regression models. Our research results using two different statistic methods, MLR and PLSR, have revealed that the QSAR equation was also improved and the predictive ability of the models was enhanced with the increase of the variable. Eg.5 is built on KB-A1 cell line with a cytotoxic compound of $2.5\mu\text{M}$ ADR while Eg.6 is based on P388/VDR-20 cell line with $1.5\mu\text{M}$ VCR. Here, most of the models gave satisfactory cross-validated Q^2 above 0.500, conventional R above 0.800 and less SE values indicating their proper predictive ability. Significant differences between values were examined using two-tailed paired T test provided by SPSS. All the results were considered not significant if $P < 0.05$. Eg.5 model is the most significant and indicated that the capability of P-gp modulators interacted with P-gp depends upon MR, BI, E_{hyd} , ShA, and LogP. The former three display positive contributions to the MDR activity of P-

gp, suggesting that the MDR activity increase accordingly with MR increase. The latter two displays negative contribution to the MDR activity of P-gp.

On the other hand, we have built the predicted models for K_a of ATPase of some compounds using the same statistic methods in order to get a more accurate model. Both models, Eg.11 by MLR and Eg.12 by PLSR, point out that LogP and E_{HOMO} are both important parameters with the affinity for and simulation of the P-gp ATPase. LogP is negative related with the activity of P-gp ATPase, suggesting that the ATPase activity also decrease with the increase of LogP. Figure 3 showed that molecular A39 and A42 have higher K_a value of ATPase and is a departure from other compounds. This may be because they have lower lipophilicity, which is supported by the research results of Diethart Schmid et al (1999). Another significant descriptor E_{HOMO} is positive related with the activity of P-gp ATPase.

In another aspect, BBB partitioning is mainly found to depend upon two parameters, namely PSA and ClogP. With the increase of the variable, the relativity of QSAR equation is also improved, and the predictive ability of the model is enhanced, especially Eq.18 most significant. Moreover, the BBB partitioning measures of the test set compounds were predicted with the same accuracy as the compounds of the training set. The family of these QSAR models reveal that the capability of BBB partitioning of an organic compound focus on six significant features, which are PSA, ClogP, BI, E_{stretch} , ΔE_{total} , and $\Delta E_{\text{torsion}}$ (Eg. 18). Obviously, two of the six descriptors of the QSAR models have positive regression coefficients and the other four descriptors have negative regression coefficients. The potential of an organic compound through BBB is directly proportional to ClogP and ΔE_{total} , but inversely proportional to PSA, BI, E_{stretch} and $\Delta E_{\text{torsion}}$. Moreover, PSA descriptor is found as a dominant descriptor in these QSAR models, which related to the aqueous solubility of the solute compound along with a direct lipophilicity descriptor (Clark et al, 1999). When the value of PSA of a molecule lessens within the range from 0 to 108.80 \AA^2 , its value of LogBB will increase. This is consistent with the experimental results that the more polarity it possesses, the more difficultly a molecule enters the hydrophobic environment of BBB (Stouch, 1993). BI is the connective index of molecular average total distance, which pertains to the volume parameter. Our research result points it out that with the accretion of its bulk, a molecule more and more difficultly across through BBB by diffusion. However, the value of LogBB of a molecule increases with the increase of ClogP. It means that the hydrophobic molecule can pass through BBB more easily than the hydrophilic molecule does, which is supported by the experimental results (Kaliszan & Markuszewski, 1996). The presence of E_{stretch} descriptor suggests that with the decrease of the stretch-bend energy of a molecule, its value of LogBB increases. Two of the descriptors, found in the log BB QSAR models (Eg.17 and Eq.18), reflect the behavior of the solute in the membrane and the entire membrane-solute complex. Along with the meaning mentioned, ΔE_{total} is equivalent to the change in average total potential energy between the triple member complex and the double member complex. Similarly, $\Delta E_{\text{torsion}}$ is the difference between the dihedral torsion energy of the triple complex and that of the double complex. Here, the more the change value of ΔE_{total} is, the more its value of LogBB increases. This is because small molecule across BBB membrane leads to the change of the structure of the complex. The more changeability of the structure results in greater change of total potential energy, while the accretion of the energy change is the important cause of the increase of the capability of a small molecule through BBB. On the contrary, the less the difference of the torsion energy is, the

larger its value of LogBB is. It displays that a small molecule tight combining with the membrane-water complex leads to increase its value of LogBB. And the relationship would suggest that as the solute becomes more flexible within the membrane-water complex, the greater would be its log BB value, which is in agreement with the research results of Iyer M et al (2002).

Several non-MI-QSAR computational models to describe and predict BBB partitioning have been reported that includes other descriptors besides PSA and ClogP (Lombardo et al, 1996; Keseru & Molnar, 2001; Crivori et al, 2000). An alternative, complementary approach to BBB partitioning prediction uses MI-QSAR analysis developed by Iyer M et al (2002). Their research results show that BBB partitioning of an organic compound depend upon PSA, CLogP, and the conformational flexibility of the compounds as well as the strength of their "binding" to the model biologic membrane. The MI-QSAR models indicate that BBB partitioning process can be reliably described for structurally diverse molecules provided interactions of the molecule with the phospholipide-rich regions of cellular membranes are explicitly considered. An extension of these approaches that combines QSAR with solute-membrane-water complex has been developed by us, which is addition of a layer of water on the hydrophilic side of DMPC monolayer membrane in our research. And so, it is more analogous to the truth BBB environment. Our results reveal that the distribution of organic molecules through BBB was not only influenced by the properties of organic solutes, but also related to the property of the solute-membrane-water complex. The former involves the polarity, hydrophobic, size, and conformational freedom degree of organic molecules. The latter deals with the strength of an organic molecule combined with BBB membrane and the structural changeability of a solute-membrane-water complex. Furthermore, the capability of a small molecule across BBB is mainly related to four physicochemical factors, which depend on the relative polarity of a small molecule, the molecular volume, the strength of a small molecule combined with DMPC-water model, and the changeability of the structure of a solute-membrane-water complex. The relative polarity of a small molecule includes two parameters, namely PSA and ClogP. The QSAR model shows that less polarity and more hydrophobic molecules relatively easily pass through BBB and enter brain to cure. The molecular volume involves one parameter, namely BI. The strength of a small molecule combined with DMPC monolayer membrane complex with a layer of water involves one parameter, namely $\Delta E_{\text{torsion}}$. The changeability of the structure of a complex between a small molecule and the membrane-water complex includes one parameter, namely ΔE_{total} . The reason for the change of total energy is that small molecule across BBB membrane leads to the change of the structure of the solute-membrane-water complex. The more the changeability of the complex structure is, the more the change value of total energy is, and the more easily a small molecule penetrates BBB.

Cerebral clearance of A β is considered to occur via elimination across BBB, as well as proteolytic degradation. Attenuation of its elimination is likely to result in increased cerebral A β deposition, which may facilitate progression of AD (Ohtsuki et al, 2010). P-gp detoxifies cells by exporting hundreds of chemically unrelated toxins but has been implicated in MDR in the treatment of cancers. Substrate promiscuity is a hallmark of P-gp activity, thus a structural description of poly-specific drug-binding is important for the rational design of anti-amyloid accumulation drugs, anticancer drugs and MDR inhibitors. The x-ray structure of apo P-gp at

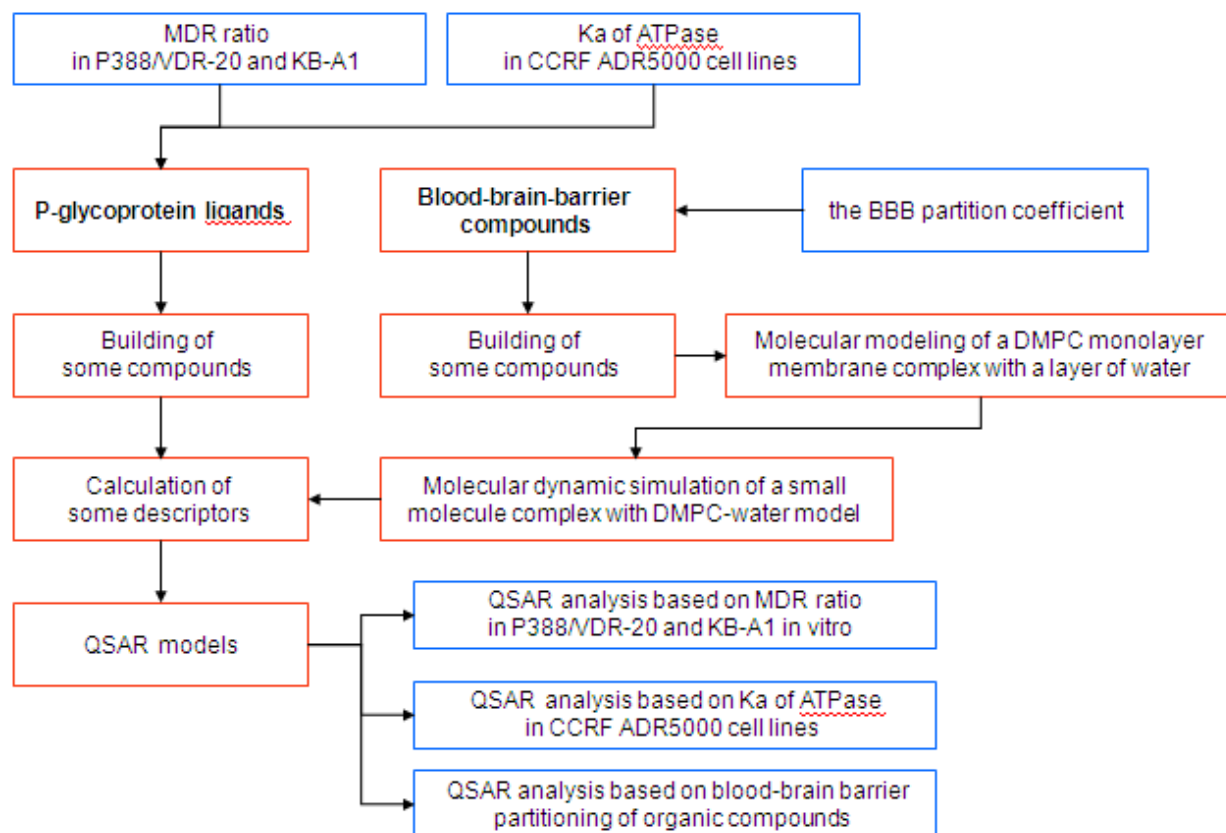
3.8 angstroms reveals an internal cavity of approximately 6000 angstroms cubed with a 30 angstrom separation of the two nucleotide-binding domains. Two additional P-gp structures with cyclic peptide inhibitors demonstrate distinct drug-binding sites in the internal cavity capable of stereoselectivity that is based on hydrophobic and aromatic interactions. Apo and drug-bound P-gp structures have portals open to the cytoplasm and the inner leaflet of the lipid bilayer for drug entry. The inward-facing conformation represents an initial stage of the transport cycle that is competent for drug binding (Aller et al, 2009). Currently, P-gp is identified as an energy-dependent pump, ATPase activity as an assay in itself is possibly problematical cause it is based upon one assumption that drug-induced ATP hydrolysis reflects transport by the transporter (Stouch & Gudmundsson, 2001). There may be many ways in which this activity could be altered, including direct action on the ATP binding domain. Scientists once observed some compounds such as daunomycin and vinblastine inhibit ATPase activity, but increase in others, suggesting that modulation of ATPase activity is highly dependent on experimental conditions and may not correlate well with the ability of P-gp to transport the drug (Ambudkar et al, 1992; Shapiro & Ling, 1994; Doige et al, 1993). The work of Litman et al was one of the few studies suggesting that affinity between drugs and ATPase activity has no correlation to LogP, but Surface Area (Litman et al, 1997). Because of the less comparability of molecular structures in a training set, our QSAR equation possesses universal significance. However, the precision of QSAR equation is so low that there is still a distance to its application. So a series of organic compounds with similar structures are chosen and consist of a training set, thus the precision of QSAR simulation is largely increased, while the prediction of the analogues through BBB is greatly improved.

5. Conclusion

P-gp is involved in MDR and in neurodegenerative disorders such as Parkinson disease, AD and epilepsy. The xenobiotic efflux pump P-gp limits intracellular drug accumulation by active extrusion of compounds out of cells. P-gp mediates the efflux of A β from the brain together with mediating MDR, while P-gp transports neutral or positively-charged hydrophobic substrates with consuming energy from ATP hydrolysis. We have built up theoretical models of the interaction between organic compounds and P-gp and compounds with the affinity for and simulation of the P-gp ATPase. The interaction between compounds and p-gp (P-gp binding or MDR-reversal activity of compounds) is found to depend on LogP, LogMR, and ShA of compounds it transports, which proportional to LogMR while inversely proportional to LogP and ShA (see Eg.1 to Eg.5). Until now we have not convinced that ATPase activity of P-gp is well correlated with the ability of P-gp to transport the drugs. However, our constructed model based on the analogies of purine and propafenone analogs suggests that the enzyme hydrolysis of these compounds largely depends on LogP, MR, ShA, MW and E_{HOMO} , especially positive related to MR but negative to LogP and ShA (see Eg.7 to Eq.11). This shows that the P-gp binding capacity of these compounds shares common characteristics with their ATPase hydrolysis, namely their hydrophobic parameters (such as log P) and steric parameters (eg. MW, ShA, MR, and WI).

Additionally, our constructed MI-QSAR model indicates that the distribution of organic molecules through BBB was not only influenced by organic solutes themselves, but also related to the properties of the solute-membrane water complex, namely interactions of the molecule with the phospholipide-rich regions of cellular membranes. Moreover, our results reveal that the ability of organic molecules permeating across BBB is proportional to LogP but inversely proportional to PSA (see Eg.13 to 18), which is consistent with the research results of Chen and co-worker (2009), namely the increasing PSA decreased LogBB rapidly while LogP positively related to LogBB. It indicates that molecules with higher lipophilic will be partitioned into the lipid bilayer more easily with more chances to penetrate BBB, supported by the research result of Wang et al (2003), namely a large number of structurally and functionally diverse compounds as substrates or modulators of P-gp mostly sharing common structural features, such as aromatic ring structures and high lipophilicity. PSA of CNS active drug should be lower than 90 \AA^2 (Chen et al, 2009), while the penetration through the BBB is optimal for LogP value in the range 1.5–2.7 (Norinder & Haerberlein, 2002).

In comparison with the ability of organic molecules permeating across BBB, P-gp binding or MDR-reversal activity of compounds has a negative correlation with LogP. There are two reasons for this phenomenon. Firstly, the compounds with higher liposolubility are more vulnerable to cytochrome P450 metabolism, leading to faster clearance (Waterhouse, 2003). P450 enzymes (CYP450s) catalyze the metabolism of a wide variety of endogenous and



Scheme 1. Flowchart for QSAR analysis of some substrates of P-glycoprotein targeting β -amyloid clearance.

exogenous compounds including xenobiotics, drugs, environmental toxins, steroids, and fatty acids. Aminated thioxanthenes have recently been reported as P-gp inhibitors as well as its interaction with cytochrome P450 3A4 (CYP3A4), as many substrates of P-glycoprotein and CYP3A4 are common (Palmeira et al, 2012). The second reason is related to the mechanism of P-gp action. According to model proposed by Higgins and Gottesman (1992), after entering into the phospholipid bilayer, compound may interact with P-gp in the inner leaflet of the lipid bilayer. Upon interaction with P-gp, the compound is flipped from the inner leaflet to the outer leaflet of the lipid bilayer. The lipophilic compounds with high LogP enter into cellular membrane easily and intend to retain there, so its opportunity to interact with P-gp increases. The LogP not only offers opportunity to penetrate the lipid bilayer, but also gives favorable contribution to binding with protein, such as P450, P-gp.

In conclusion, the predictive model of BBB partitioning of organic compounds contributes to discovery of some molecules through BBB as potential AD therapeutic drugs. Moreover, the interaction model of P-gp and modulators for treatment of multidrug resistance indicates discovery of some molecules to increase A β clearance from the brain and reduce A β brain accumulation by regulate BBB P-gp in the early stages of AD. The mechanism suggests new therapeutic strategy in AD.

Acknowledgements

This work was supported by a grant from Basic Scientific Research Expenses of Central University (020814360012), National Key Technology R&D Program (2008BAI51B01) and Specialized Research Fund for the Doctoral Program of Higher Education (20120091110038).

Author details

Jie Yang* and Jie Chen

*Address all correspondence to: luckyjyj@sina.com.cn

State Key Laboratory of Pharmaceutical Biotechnology, Life College, Nanjing University, Nanjing, China

References

- [1] Abraham, M. H, Chadha, H. S, & Mitchell, R. C. (1995). Hydrogen bonding. 36. Determination of blood-brain barrier distribution using octanol-water partition coefficients. *Drug Des Discov* (Nov 1995), 1055-9612, 13(2), 123-131.

- [2] Abraham, M. H, Takacs-novak, K, & Mitchell, R. C. (1997). On the partition of ampholytes: Application to blood-brain distribution. *J Pharm Sci* (Mar 1997), 0022-3549, 86(3), 310-315.
- [3] Abuznait, A. H, Cain, C, Ingram, D, Burk, D, & Kaddoumi, A. (2011). Up-regulation of P-glycoprotein reduces intracellular accumulation of beta amyloid: investigation of P-glycoprotein as a novel therapeutic target for Alzheimer's disease. *J Pharm Pharmacol.* (Aug 2011), 0022-3573, 63(8), 1111-1118.
- [4] Alka, K. (2003). C-QSAR: a database of 18000 QSARs and associated biological and physical data. *J Comput Aided Mol Des* (Feb-Apr 2003), 1573-4951, 17(2-4), 187-196.
- [5] Aller, S. G, Yu, J, Ward, A, Weng, Y, Chittaboina, S, Zhuo, R, Harrell, P. M, Trinh, Y. T, Zhang, Q, Urbatsch, I. L, & Chang, G. (2009). Structure of P-glycoprotein reveals a molecular basis for poly-specific drug binding. *Science.* (Mar 2009), 0036-8075, 323(5922), 1718-1722.
- [6] Ambudkar, S. V, Dey, S, Hrycyna, C. A, Ramachandra, M, Pastan, I, & Gottesman, M. M. (1999). Biochemical, cellular, and pharmacological aspects of the multidrug transporter. *Annu. Rev. Pharmacol. Toxicol.* (Apr 1999), 0362-1642, 39, 361-398.
- [7] Ambudkar, S. V, Lelong, I. H, Zhang, J, Cardarelli, C. O, Gottesman, M. M, & Pastan, I. (1992). Partial purification and reconstitution of the human multidrug-resistance pump: characterization of the drug-stimulatable ATP hydrolysis. *Proc. Natl. Acad. Sci. USA* (Sep 1992), 0027-8424, 89(18), 8472-8476.
- [8] Bartels, A. L. (2011). Blood-brain barrier P-glycoprotein function in neurodegenerative disease. *Curr Pharm Des.* 1381-6128, 17(26), 2771-2777.
- [9] Bassolino-klimas, D, Alper, H. E, & Stouch, T. R. (1993). Solute diffusion in lipid bilayer membranes: an atomic level study by molecular dynamics simulation. *Biochemistry.* (Nov 1993), 0006-2960, 32(47), 12624-12637.
- [10] Bendayan, R, Lee, G, & Bendayan, M. (2002). Functional expression and localization of p-glycoprotein at the blood brain barrier. *Microsc. Res. Tech.*, (Jun 2002), 0105-9910X., 57(5), 365-380.
- [11] Chen, C, & Yang, J. (2006). MI-QSAR models for prediction of corneal permeability of organic compounds. *Acta Pharmacologica Sinica.* (Feb 2006), 1745-7254, 27(2), 193-204.
- [12] Chen, L. J, Lian, G. P, & Han, L. J. (2007). Prediction of human skin permeability using artificial neural network (ANN) modeling. *Acta Pharmacologica Sinica,* (Apr 2007), 1745-7254, 28(4), 591-600.
- [13] Chen, Y, Zhu, Q. J, Pan, J, Yang, Y, & Wu, X. P. (2009). A prediction model for blood-brain barrier permeation and analysis on its parameter biologically. *Comput Methods Programs Biomed.*, (Sep 2009), 0169-2607, 95(3), 280-287.
- [14] Cheng, Z, Zhang, J, Liu, H, Li, Y, Zhao, Y, & Yang, E. (2010). Central nervous system penetration for small molecule therapeutic agents does not increase in multiple scler-

- rosis- and Alzheimer's disease-related animal models despite reported blood-brain barrier disruption. *Drug Metab Dispos.* (Aug 2010), 0090-9556, 38(8), 1355-1361.
- [15] Cramer, R. D, Patterson, D. E, & Bunce, J. D. (1988). Comparative molecular field analysis (CoMFA). 1. Effect of shape on binding of steroids to carrier proteins. *J. Am. Chem. Sci.* (Aug 1988), 0002-7863, 110(18), 5959-5967.
- [16] Dhainaut, A, Regnier, G, Tizot, A, Pierre, A, Leonce, S, Guilbaud, N, Kraus-berthier, L, & Atassi, G. (1996). New purines and purine analogs as modulators of multidrug resistance. *J. Med. Chem.* (Sep 1996), 0223-5234, 39(20), 4099-4108.
- [17] Doige, C. A, Yu, X, & Sharom, F. J. (1993). The effects of lipids and detergents on ATPase-active P-glycoprotein. *Biochim. Biophys. Acta* (Feb 1993), 0006-3002, 1146(1), 65-72.
- [18] Ford, J. M, Bruggemann, E. P, Pastan, I, Gottesman, M. M, & Hait, W. N. (1990). Cellular and biochemical characterization of thioxanthenes for reversal of multidrug resistance in human and murine cell lines. *Cancer Res.* (Mar 1990), 0008-5472, 50(6), 1748-1756.
- [19] Fromm, M. F. (2004). Importance of P-glycoprotein at blood-tissue barriers. *Trends Pharmacol Sci.* (August 2004), 0165-6147, 25(8), 423-429.
- [20] Gottesman, M. M, & Pastan, I. (1993). Biochemistry of Multidrug Resistance Mediated by the Multidrug Transporter, *Annu Rev Biochem* No. (July 1993), 0066-4154, 62, 385-427.
- [21] Hartz, A. M, Miller, D. S, & Bauer, B. (2010). Restoring blood-brain barrier P-glycoprotein reduces brain amyloid-beta in a mouse model of Alzheimer's disease. *Mol Pharmacol.* (May 2010), 0002-6895X., 77(5), 715-723.
- [22] Higgins, C. F, & Gottesman, M. M. (1992). Is the multidrug transporter a flippase? *Trends. Biol. Sci.*, 0962-8924, 17, 18-21.
- [23] Iyer, M, Mishra, R, Han, Y, & Hopfinger, A. J. (2002). Predicting Blood-Brain Barrier Partitioning of Organic Molecules Using Membrane-Interaction QSAR Analysis. *Pharmaceutical Res* Nov 2002), 0724-8741, 19(11), 1611-1621.
- [24] Jabeen, I, Pleban, K, Rinner, U, Chiba, P, & Ecker, G. F. (2012). Structure-activity relationships, ligand efficiency, and lipophilic efficiency profiles of benzophenone-type inhibitors of the multidrug transporter p-glycoprotein. *J. Med. Chem.* Apr 2012), 0223-5234, 55(7), 3261-3273.
- [25] Jeynes, B, & Provias, J. (2011). An investigation into the role of P-glycoprotein in Alzheimer's disease lesion pathogenesis. *Neurosci Lett.* Jan 2011), 0168-0102, 487(3), 389-393.

- [26] Kast, C, Canfield, V, Levenson, R, & Gros, P. (1996). Transmembrane organization of mouse P-glycoprotein determined by epitope insertion and immunofluorescence. *J Biol Chem.* Apr 1996), 0021-9258, 271(16), 9240-9248.
- [27] Karelson, M. (2000). *Molecular Descriptors in QSAR/ QSPR*; John Wiley & Sons: New York. 0-47135-168-7
- [28] Karelson, M, Lobanov, V. S, & Katritzky, A. R. (1996). Quantum-chemical descriptors in QSAR/QSPR studies. *Chem. Rev.* May 9), 0003-6021X., 96(3), 1027-1044.
- [29] Kothandan, G, Gadhe, C. G, Madhavan, T, Choi, C. H, & Cho, S. J. (2011). Docking and 3D-QSAR (quantitative structure activity relationship) studies of flavones, the potent inhibitors of p-glycoprotein targeting the nucleotide binding domain. *Eur J Med Chem.* Sep 2011), 0223-5234, 46(9), 4078-4088.
- [30] Kubinyi, H. (1995). Strategies and recent technologies in drug discovery. *Pharmazie.* Oct 1995), 0031-7144, 50(10), 647-662.
- [31] Kuo, C. L, Assefa, H, Kamath, S, Brzozowski, Z, Slawinski, J, Saczewski, F, Buolamwini, J. K, & Neamati, N. (2004). Application of CoMFA and CoMSIA 3D-QSAR and docking studies in optimization of mercaptobenzenesulfonamides as HIV-1 integrase inhibitors. *J Med Chem.* Jan 2004), 0223-5234, 47(2), 385-399.
- [32] Li, Y, Wang, Y. H, Yang, L, Zhang, S. W, Liu, C. H, & Yang, S. L. (2005). Comparison of steroid substrates and inhibitors of P-glycoprotein by 3D-QSAR analysis. *J. Mol. Struct.* Sep 2005), 0166-1280, 733(1-3), 111-118.
- [33] Litman, T, Zeuthen, T, Skovsgaard, T, & Stein, W. D. (1997). Structure-activity relationships of P-glycoprotein interacting drugs: kinetic characterization of their effects on ATPase activity, *Biochem. Biophys. Acta* Aug 1997), 0006-3002, 1361(2), 159-168.
- [34] Ma, X. L, Chen, C, & Yang, J. (2005). Predictive model of blood-brain barrier penetration of organic compounds. *Acta Pharmacologica Sinica.* Apr 2005), 1745-7254, 26(4), 500-512.
- [35] Norinder, U, & Haeberlein, M. (2002). Computational approaches to the prediction of the blood-brain distribution. *Adv Drug Deliv Rev.*, (Mar 2002):291-313, 0016-9409X., 54(3)
- [36] Ohtsuki, S, Ito, S, & Terasaki, T. (2010). Is P-glycoprotein involved in amyloid- β elimination across the blood-brain barrier in Alzheimer's disease? *Clin Pharmacol Ther.* (Oct 2010), 0009-9236, 88(4), 443-445.
- [37] Ooms, F, Wouters, J, Collin, S, Durant, F, Jegham, S, & George, P. (1998). Molecular lipophilicity potential by CLIP, a reliable tool for the description of the 3D distribution of lipophilicity: application to 3-phenyloxazolidin-2-one, a prototype series of reversible MAOA inhibitors. *Bioorg. Med. Chem. Lett.* (Jun 1998), 0096-0894X., 8(11), 1425-1430.

- [38] Palmeira, A, Sousa, E, Fernandes, M. X, Pinto, M. M, & Vasconcelos, M. H. (2012). Multidrug resistance reversal effects of aminated thioxanthenes and interaction with cytochrome P450 3A4. *J Pharm Pharm Sci.*, (Jan 2012), 1482-1826, 15(1), 31-45.
- [39] Ponce, Y. M, Garit, J. A, Torrens, F, Zaldivar, V. R, & Castro, E. A. (2004). Atom, atom-type, and total linear indices of the "molecular pseudograph's atom adjacency matrix": application to QSPR/QSAR studies of organic compounds. *Molecules* (Dec. 31), 1420-3049, 9(12), 1100-1123.
- [40] Schmid, D, Ecker, G, Kopp, S, Hitzler, M, & Chiba, P. (1999). Structure-activity relationship studies of propafenone analogs based on P-glycoprotein ATPase activity measurements. *Biochem Pharmacol.* (Nov 1999), 0300-5127, 58(9), 1447-1456.
- [41] Shapiro, A. B, & Ling, V. (1994). ATPase activity of purified and reconstituted P-glycoprotein from Chinese hamster ovary cells. *J. Biol. Chem.* (Feb 1994), 0021-9258, 269(5), 3745-3754.
- [42] Sharom, F. J. (1997). The P-Glycoprotein Efflux Pump: How Does it Transport Drugs? *J. Membr. Biol.* (Dec 1997), 0022-2631, 160(3), 161-175.
- [43] Stouch, T. R, & Gudmundsson, O. (2002). Progress in understanding the structure-activity relationships of P-glycoprotein. *Adv Drug Deliv Rev.* (Mar 2002), 0016-9409X., 54(3), 315-328.
- [44] Taub, M. E, Podila, L, Ely, D, & Almeida, I. (2005). Functional assessment of multiple P-glycoprotein (P-gp) probe substrates: influence of cell line and modulator concentration on P-gp activity. *Drug Metab Dispos.* (Nov 2005), 0090-9556, 33(11), 1679-1687.
- [45] Vogelgesang, S, Jedlitschky, G, Brenn, A, & Walker, L. C. (2011). The role of the ATP-binding cassette transporter P-glycoprotein in the transport of β -amyloid across the blood-brain barrier. *Curr Pharm Des.* 171381-6128(26), 2778-2786.
- [46] Wang, R. B, Kuo, C. L, Lien, L. L, & Lien, E. J. (2003). Structure-activity relationship: analyses of p-glycoprotein substrates and inhibitors. *J Clin Pharm Ther.* (Jun 2003), 0269-4727, 28(3), 203-228.
- [47] Wang, Y. H, Li, Y, Yang, S. L, & Yang, L. (2005). An in silico approach for screening flavonoids as P-glycoprotein inhibitors based on a Bayesian-regularized neural network. *J Comput Aided Mol Des.* (Mar 2005), 0092-0654X., 19(3), 137-147.
- [48] Wang, Y. H, Li, Y, Yang, S. L, & Yang, L. (2005). Classification of Substrates and Inhibitors of P-Glycoprotein Using Unsupervised Machine Learning Approach. *J. Chem. Inf. Model.* (May 2005), 1549-9596, 45(3), 750-757.
- [49] Waterhouse, R. N. (2003). Determination of lipophilicity and its use as a predictor of blood-brain barrier penetration of molecular imaging agents. *Mol Imaging Biol.*, (Nov-Dec 2003), 1536-1632, 5(6), 376-389.

- [50] Wiese, M, & Pajeva, I. K. (2001). Structure-Activity Relationships of Multidrug Resistance Reversers. *Curr. Med. Chem.* (May 2001), 0929-8673, 8(6), 685-713.

IntechOpen

IntechOpen

